ISSN 1590-8844
International Journal of Mechanics and Control, Vol. 23, No. 01, 2022

OPTIMAL OPERATION OF POWER-SPLIT HYBRID ELECTRIC POWERTRAIN: COMPARISON BETWEEN TWO PERFORMANCE INDICES

Antonella Castellano* Marco Cammalleri*

* University of Palermo, Department of Engineering, 90128 Palermo, Italy

ABSTRACT

Among all the current environmentally-friendly ground vehicles proposed to reduce fuel consumption and emissions, power-split hybrid electric vehicles represent one of the most promising solutions. Their operation is based on the cooperation of the thermal engine and the electric unit enabled by mechanical transmissions consisting of planetary and ordinary gear sets. However, implementing proper energy management strategies to realise the best powertrain operations is crucial to maximise the environmental gain without compromising performance and drivability. For this purpose, an initial comprehensive analysis of the powertrain response is required. In this respect, this paper relies on a unified parametric approach, available in the literature, to investigate the acceleration response of an output-split hybrid electric powertrain by also considering the transmission mechanical power losses. The efficiency maps of the engine and electric machines are introduced to assess two performance indices. These are the powertrain real global efficiency and a fictitious equivalent efficiency where the efficiency of each actuator is normalised to the respective maximum value. The aim is to compare the optimal powertrain operation resulting from the maximisation of each performance index for a given vehicle speed and acceleration.

Keywords: hybrid electric vehicles, power-split powertrain, PS-CVT analysis, model-based optimisation, SDG13.

1 INTRODUCTION

So far, several governments worldwide have adopted relevant environmental policies to face climate change. Significant economic stimulus on Hybrid Electric Vehicles (HEVs) purchase has been promoted to reduce greenhouse gases and toxic emissions while waiting for the ultimate establishment of pure electric vehicles. Indeed, the cooperation of the thermal engine and the electric unit allows HEVs to overcome some technological downsides of pure electric vehicles, such as range anxiety and charging time, emitting much less than conventional engine-based vehicles.Several architectures of HEVs are currently available on the market, differing for the degree of hybridisation and functional layout [1–4].

Contact author: Antonella Castellano[1], Marco Cammalleri[2]
E-mail:
antonella.castellano@unipa.it; marco.cammalleri@unipa.it

The higher level of electrification of Full Hybrid Electric Vehicles (FHEVs) increases fuel-saving and reduces emissions compared with micro and mild hybrid performance. The possibility to recharge the battery directly from the grid available on Plug-in Hybrid Electric Vehicles (PHEVs) drastically decreases local emissions even more. Among the HEVs layouts, the power-split architecture is the most promising one over series and parallel hybrid [5, 6]. The Internal Combustion Engine (ICE) cooperates with an electric unit consisting of two electric machines, power converters and batteries. The deployment of Planetary Gear sets (PGs) and Ordinary Gear sets (OGs), properly arranged in a Power-Split Unit (PSU), enables the decoupling of the thermal engine operation from the wheels speed to work in the most efficient region. Therefore, the electric unit operates as a Continuously Variable Unit (CVU), but it can also fulfil power demand partially, supporting the ICE, or entirely for the full-electric drive. The counterpart of the enhanced flexibility of operation of the power-split hybrid powertrain is the increased complexity in design and control compared to series and parallel layouts.

Several Energy Management Strategies (EMSs) have been developed to effectively select the optimal power ratio between the ICE and the electric unit that minimises fuel consumption while maintaining satisfactory performance and the desired battery State Of Charge (SOC) [7–15]. A broad research trend focuses on model-based EMSs, such as Equivalent Consumption Minimisation Strategy (ECMS) or Model Predictive Control (MPC), which show the potential to reduce computational effort and be implemented in real-time. Nonetheless, the plant model embedded in the control strategy should reproduce the powertrain behaviour as accurately as possible, thus considering the conversion power losses in the ICE and electric machines and the transmission mechanical power losses. The efficiency of the power sources can be easily assessed from the respective efficiency maps. On the contrary, evaluating the mechanical power losses in the PSU is far from trivial [16–18].

Moreover, different control strategies should be adopted for FHEVs and PHEVs since battery recharge from the grid available in PHEVs enables driving in a charge-depleting mode, in contrast to FHEVs that only allow a charge-sustaining drive [9, 12, 15]. Thus, the cost function minimised by the EMS should be defined accordingly to the powertrain characteristics to enhance fuel saving while maintaining the battery SOC within the desired range. Nonetheless, different cost functions deeply affect the resulting optimised operation of the powertrain [19].

The objective of this paper is to compare two different performance indices to optimise. These are the powertrain real global efficiency and a fictitious equivalent efficiency conceived to consider the notable differences between ICE and electric machines operations. The aim is to show how the optimal powertrain operations are affected by the objective function to maximise. The analysis relies on a parametric model, described in [20–23], which enables the evaluation of the mechanical power losses occurring in the PSU for higher model accuracy.

This paper expands the study proposed in [24], where the steady-state response of a power-split powertrain was investigated and the operating points leading to the best global efficiency were selected. In the following, the same output-split powertrain is analysed by a backward approach considering also vehicle acceleration. Section 2 summarises the dimensionless parametric model underpinning the analysis, which can assess the speed and power ratios between the wheels, the ICE and the electric machines. It includes a fast approximate method to evaluate the PSU mechanical power losses [22, 23]. Section 3 defines the performance indices taken into consideration in this study and the procedure for their evaluation. A simplified approach assuming four different scenarios is adopted to model the battery SOC. The study results are provided in Section 4, where a comparison between the two performance indices is discussed, while Section 5 concludes the paper.

2 DIMENSIONLESS PARAMETRIC MODEL FOR POWER-SPLIT TRANSMISSIONS

Power-Split Continuously Variable Transmissions (PS-CVTs) are classified into shunt or compound PS-CVTs, depending on the number of planetary gear sets, that can be one or more, respectively. Shunt PS-CVTs are divided into input-split and output-split, where one electric machine speed is proportional to the wheels speed or to the engine speed, respectively. Moreover, compound PS-CVTs often include a clutch system to switch between several operating modes, realising multimode power-split transmissions. Nevertheless, the unified parametric model addressed in [20–23] can model any PS-CVT, regardless of PGs number and arrangement, as a black box comprehensively characterised by some functional parameters identifiable from the transmission constructive layout by the procedure described in [23]. Figure 1 shows a schematic representation of any PSU, which has four external ports linked to the ICE (*in*), the wheels (*out*) and the electric Motor-Generators (MGs) I and O (*i* and *o*).

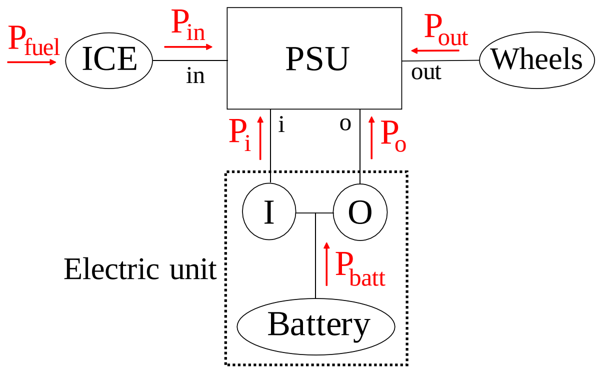

Figure 1 PS-CVTs schematisation as a black box with the positive sign for power flows.

The functional parameters necessary to implement the model are the so-called nodal ratios and the corresponding speed ratios. The former, indicated as $\tau_{\#k}$, are the overall speed ratio $\tau = \omega_{out}/\omega_{in}$ achieved when a generic kth shaft is motionless. The latter, indicated as $\tau_{j\#k}$, are the jth speed ratio $\tau_j = \omega_j/\omega_{in}$ calculated for the kth nodal ratio. Once these functional parameters are identified, they lead to the assessment of the speed and power ratios between the PSU ports. Indeed, since the PSU has two degrees of freedom, all the relationships are normalised to ICE speed and power to reduce the mathematical treatment to a problem with a single degree of freedom. Moreover, the whole model can be rearranged to address full electric operation [23, 25]. All the significant relations essential to the model comprehension are summarised in section 2.2, while the application of the model to the output-split transmission under analysis is carried out in Section 2.2.

ISSN 1590-8844
International Journal of Mechanics and Control, Vol. 23, No. 01, 2022

2.1 SPEED AND POWER RATIOS

The kinematic relationships among the PSU external ports are expressed as functions of the overall speed ratio τ:

$$\tau_i = \frac{\omega_i}{\omega_{in}} = \tau_{i\#o} \frac{\tau - \tau_{\#i}}{\tau_{\#o} - \tau_{\#i}} \tag{1}$$

$$\tau_o = \frac{\omega_o}{\omega_{in}} = \tau_{o\#i} \frac{\tau - \tau_{\#o}}{\tau_{\#i} - \tau_{\#o}} \tag{2}$$

The ideal power ratios depend on the overall speed ratio τ and the overall power ratio $\eta = -P_{out}/P_{in}$:

$$p_i = \frac{P_i}{P_{in}} = \frac{(\tau - \tau_{\#i})(\tau - \eta\, \tau_{\#o})}{\tau(\tau_{\#i} - \tau_{\#o})} \tag{3}$$

$$p_o = \frac{P_o}{P_{in}} = \frac{(\tau - \tau_{\#o})(\tau - \eta\, \tau_{\#i})}{\tau(\tau_{\#o} - \tau_{\#i})} \tag{4}$$

Positive signs for power flows are shown in Figure 1. It should be noted that η is not an efficiency parameter, because it may also be greater than one if the demanded power is supplied not only by the ICE but also by the battery.

One of the strengths of this model is the simplicity in assessing the mechanical power losses occurring in the PSU. Indeed, a rigorous study of the PSU mechanical power losses would require the identification of the speed or torque reversals in each PG shaft, which cause discontinuities in the related mechanical loss factor. In this regard, a fast approximate procedure that ignores such discontinuities and applies to any PS-CVT was proposed [22, 23]. Once known the constructive ratio and the loss factors of PGs and OGs, the mechanical power losses occurring in the PSU can be computed as a function of τ and η. For brevity, the related theoretical background is not explained in this paper, but the reader could find more details in [22, 23], while an example of their calculation is presented in Section 2.2. The procedure outputs the total mechanical power losses normalised to the ICE power ($\bar{p}_L = \bar{P}_L/P_{in}$). From the PSU power losses, the actual mechanical power required or provided by the electric machines can be calculated by the following equations:

$$\bar{p}_i = \frac{\bar{P}_o}{P_{in}} = p_i - \frac{\tau_i}{\tau_{i_{\#o}}}\left[\bar{p}_L + \left(\frac{\partial \bar{p}_L}{\partial \tau} + \frac{\partial \bar{p}_L}{\partial \eta}\frac{\eta}{\tau}\right)(\tau_{\#o} - \tau)\right] \tag{5}$$

$$\bar{p}_o = \frac{\bar{P}_o}{P_{in}} = p_o - \frac{\tau_o}{\tau_{o_{\#i}}}\left[\bar{p}_L + \left(\frac{\partial \bar{p}_L}{\partial \tau} + \frac{\partial \bar{p}_L}{\partial \eta}\frac{\eta}{\tau}\right)(\tau_{\#i} - \tau)\right] \tag{6}$$

Note that overlined symbols indicate actual mechanical power flows. Moreover, this approach relies on the hypothesis that only the electric machines compensate for the PSU mechanical power losses; therefore, there is no distinction between P_{in} and $\bar{P}_{in}$ and between P_{out} and $\bar{P}_{out}$.

In Section 2.2, this dimensionless parametric model is applied to an output-split transmission to obtain the speed ratios, the mechanical power losses and the actual mechanical power ratios at the PSU ports.

2.2 APPLICATION TO AN OUTPUT-SPLIT CVT

The transmission under analysis is an output-split transmission designed in [26]. The constructive layout of the transmission is shown in Figure 2, where the PG is indicated with a rounded square, while rhombi indicate OGs. The PG Willis' ratio is $\Psi = \omega_R/\omega_S|_{\omega_C=0} = -0.4$, while the OGs fixed ratios are $k_{in} = \omega_{in}/\omega_R = 0.82$ and $k_{out} = \omega_{out}/\omega_C = 0.25$. *R*, *S* and *C* stand for PG Ring gear, Sun gear and Carrier, respectively.

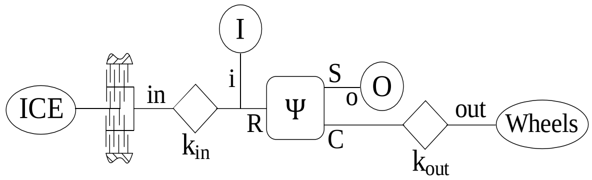

Figure 2 Output-split transmission under analysis

From this constructive arrangement, the resulting basic functional parameters are $\tau_{\#o} = 0.218$, $\tau_{\#i} = \tau_{o\#i} = -\infty$, $\tau_{i\#o} = 1.22$ [26]. The speed ratios τ_i and τ_o and the ideal power ratios p_i and p_o can be swiftly assessed by Eqs. (1)-(4). The normalised mechanical losses in the PSU can be computed by summing the power losses in the OGs and the PG, evaluated by the approximated method described in [22, 23]:

$$\bar{p}_L|_{OG_{in}} = \frac{\bar{P}_{Loss}|_{OG_{in}}}{P_{in}} \approx -\left|\left(1 - \eta_{OG_{in}}\right) p_{in}\right| \tag{7}$$

$$\bar{p}_L|_{OG_{out}} = \frac{\bar{P}_{Loss}|_{OG_{out}}}{P_{in}} \approx -\left|\left(1 - \eta_{OG_{out}}\right) p_{out}\right| \tag{8}$$

$$\bar{p}_L|_{PG} = \frac{\bar{P}_{Loss}|_{PG}}{P_{in}} \approx \approx -\left|(1 - \eta^S)\left(\frac{\phi^o_{out/i} - \psi^S_{C/R}}{1 - \psi^S_{C/R}}\right) p_{out}\right| \tag{9}$$

where $p_{in} = P_{in}/P_{in} = 1$ and $p_{out} = P_{out}/P_{in} = -\eta$. The OGs efficiency is $\eta_{OG_{in}} = \eta_{OG_{out}} = 0.98$. The parameter $\psi^S_{C/R}$ in Eq. (9) is the speed ratio between the carrier and the ring gear when the sun gear is still, while η^S is the efficiency of the PG evaluated when its sun is still. Therefore, both are constant parameters depending on the PG Willis' ratio Ψ and its fixed-carrier efficiency $\eta_0 = 0.96$:

$$\psi^S_{C/R} = \frac{1}{1 - \Psi} \tag{10}$$

$$\eta^S = \frac{1 - \Psi}{1 - \dfrac{\Psi}{\eta_0}} \tag{11}$$

$\phi^o_{out/i}$ is the so-called characteristic function, a crucial tool of this unified parametric model for both analysis and design purposes, as addressed in [20, 23]. For brevity, it is sufficient to know that it depends on the only nodal ratios and is a function of the overall speed ratio τ:

$$\phi^o_{out/i} = \frac{\tau_{\#o}}{\tau_{\#o} - \tau_{\#i}} \frac{\tau - \tau_{\#i}}{\tau} \tag{12}$$

ISSN 1590-8844
International Journal of Mechanics and Control, Vol. 23, No. 01, 2022

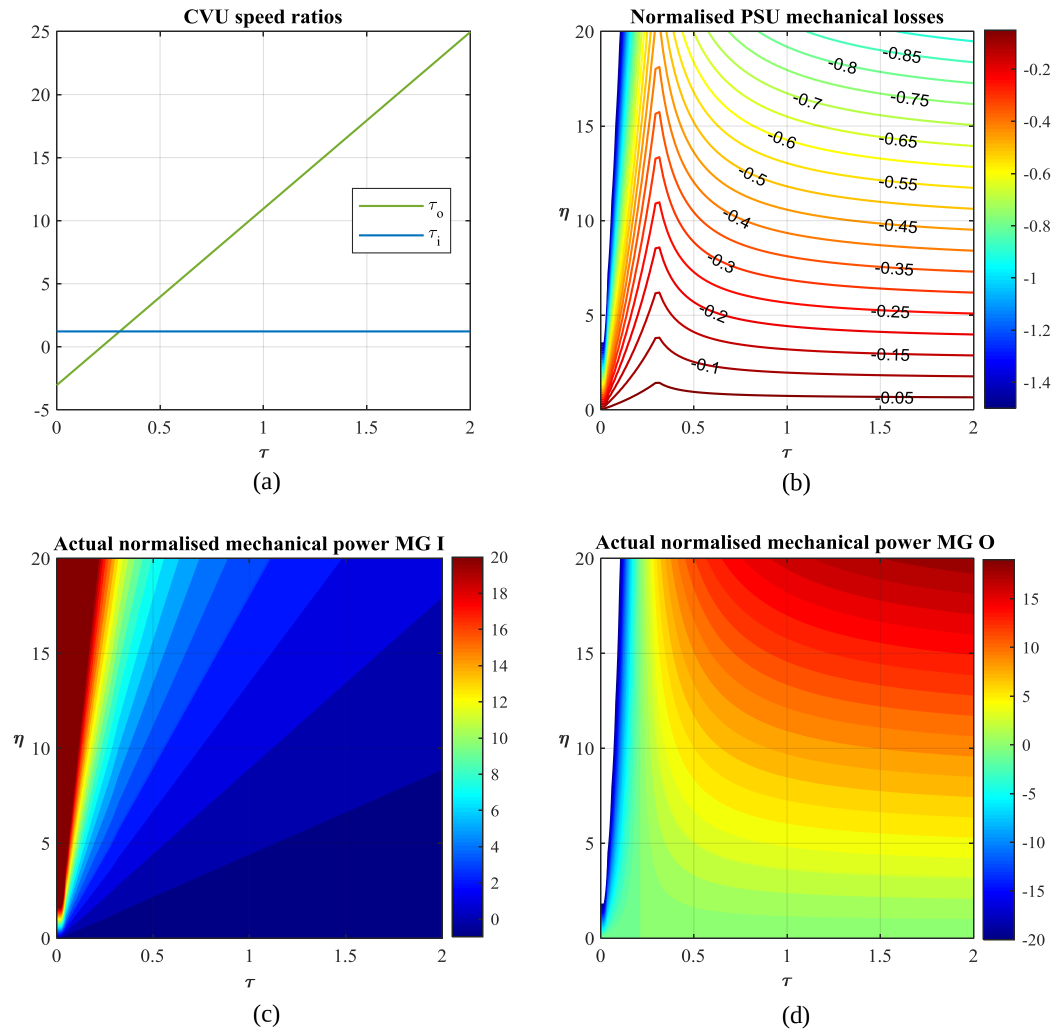

Figure 3 Results of the application of the dimensionless parametric model.

The total normalised PSU mechanical power losses are:

$$\bar{p}_L = \bar{p}_L|_{OG_{in}} + \bar{p}_L|_{OG_{out}} + \bar{p}_L|_{PG} \tag{13}$$

At this point, the actual mechanical power at the electric machines ports can be evaluated by Eqs. (5)-(6).
Figure 3 shows the results of the dimensionless analysis of the transmission in terms of CVU speed ratios (Figure 3(a)), PSU mechanical power losses (Figure 3(b)), and CVU actual mechanical powers expressed as a fraction of the input power (Figure 3(c)-(d)).

3 PERFORMANCE INDICES: DEFINITION AND ASSESSMENT

In developing optimisation-based EMSs for HEVs, the definition of an adequate cost function is of paramount importance. In general, any control strategy aims to minimise fuel consumption, which is relatively trivial in a conventional ICE-based vehicle.

In this simple case, the ICE optimisation problem is reduced to maximise engine efficiency. On the contrary, the additional energy source available in HEVs complicates the problem because the optimisation of ICE operation cannot be decoupled from the optimal management of the battery SOC. Moreover, it is challenging to consider the consumption or the gain of electric energy provided or gathered by the battery and compare it to the fuel consumption. Last but not least, developing a proper EMS is even more difficult in power-split HEVs because of the additional degrees of freedom available. This section proposes two different performance indices to maximise in order to determine the optimal powertrain operations. However, a comprehensive analysis of the powertrain response is required before assessing the performance indices. In this respect, the results obtained in Section 2.2 are not sufficient to define the conversion power losses in ICE and electric MGs because their efficiency depends on their operating points, which are still undefined.

Hence, Section 3.1 describes the procedure adopted to shift from dimensionless to dimensional variables by introducing the characteristic curves of each power source or load attached to the PSU ports.

3.1 ANALYSIS OF THE POWERTRAIN RESPONSE

The dimensionless approach summarised in Section 2 enables the comprehensive analysis of the PSU response once freely assumed a speed ratio and a power or torque ratio between any two external PSU shafts. Nonetheless, the overall speed ratio τ and the overall power ratio η were chosen as independent variables for convenience. Indeed, the output speed ω_{out} is directly related to the vehicle speed, while the output power delivered to the wheels depends on the vehicle speed (V_{veh}) and acceleration (a_{veh}), as follows:

$$P_{out}(V_{veh}, a_{veh}) = -(mg\sin\gamma + f_r mg\cos\gamma + \frac{1}{2}C_d A_f \rho_a V_{veh}^2 + ma_{veh})V_{veh} \tag{14}$$

P_{out} is negative because it is delivered by the PSU. In Eq. (14), m is the vehicle mass, $g = 9.81$ m/s^2 is the gravitational acceleration, γ is the road slope expressed in radians, f_r is the rolling resistance coefficient, C_d is the drag coefficient, A_f is the vehicle frontal area and $\rho_a = 1.225$ kg/m^3 is the air density. Table I shows the assumed values of the fixed parameters, while γ, V_{veh} and a_{veh} can vary depending on the driving conditions.

Table I - Vehicle parameters

m	2200 kg
f_r	0.0122 [-]
C_d	0.4 [-]
A_f	2.5 m2
R_w	0.3 m

For each feasible combination of V_{veh} and a_{veh}, a functioning point of the ICE has to be selected in terms of speed (ω_{in}) and torque (T_{in}) to determine the overall speed and power ratios:

$$\tau(V_{veh}, \omega_{in}) = \frac{V_{veh}}{R_w \cdot \omega_{in}} \tag{15}$$

$$\eta(V_{veh}, a_{veh}, \omega_{in}, T_{in}) = -\frac{P_{out}}{\omega_{in}T_{in}} \tag{16}$$

where R_w is the wheels radius.

The whole ICE working range must be explored to investigate all the possible powertrain functioning points for given vehicle speed and acceleration. Thus, ICE operations can be freely selected from the ICE efficiency maps (Figure 4). Each engine operating point involves a certain engine efficiency. As a result, the power supplied by the fuel can be easily calculated as well:

$$P_{fuel}(\omega_{in}, T_{in}) = \frac{\omega_{in}T_{in}}{\eta_{ICE}} \tag{17}$$

Thus, once the vehicle speed and engine operating point are fixed, the overall speed and power ratios are univocally defined and are used to interpolate the speed and power ratios of Figure 3.

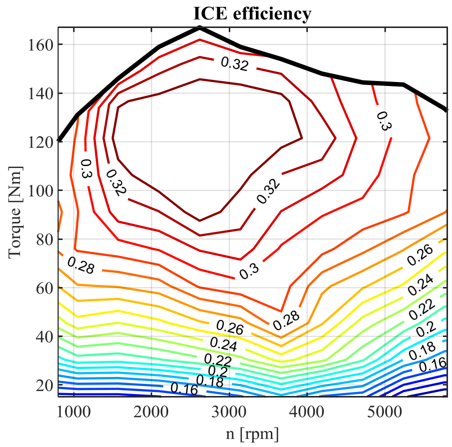

Figure 4 ICE efficiency maps.

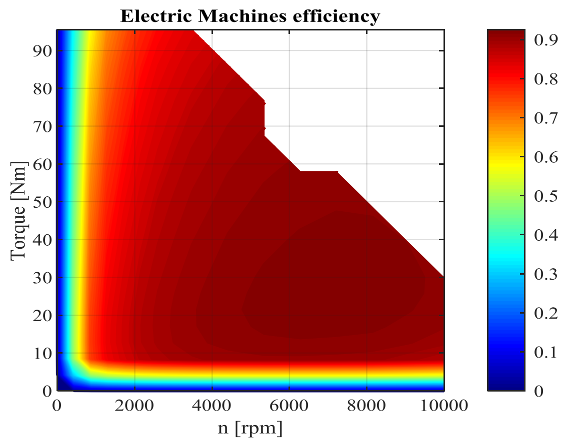

Figure 5 Electric machines efficiency maps.

Then, these ratios can be multiplied by the corresponding ω_{in} and $P_{in} = \omega_{in}T_{in}$ to assess the rotational speed of the electric machines (ω_i, ω_o) and their actual mechanical power ($\bar{P}_i$, $\bar{P}_o$). In this way, the operating point of both electric machines is determined, leading to the assessment of their efficiency from their efficiency map, shown in Figure 5. Note that MG I and MG O are identical by design [26] and that the efficiency map of Figure 5 is considered for both motoring and generating operations.

Lastly, the net electric power flowing to or from the battery is computed as follows:

$$P_{batt}(V_{veh}, a_{veh}, \omega_{in}, T_{in}) = \bar{p}_o P_{in}\eta_O^{-sign(\bar{p}_o)} + \bar{p}_i P_{in}\eta_I^{-sign(\bar{p}_i)} \tag{18}$$

The described procedure outputs a set of matrices containing all the possible powertrain operations for each combination of vehicle speed and acceleration.

These results can be used as a basis for the desired model-based EMS. By way of example, in this paper, they are used to compare the results from optimising the performance indices described in Section 3.2.

3.2 PERFORMANCE INDICES

The first performance index taken into account is the real global efficiency of the powertrain (ε_{real}), indicated as the ratio between the output power delivered to the wheels (P_{out}) and the input power provided by the fuel combustion (P_{fuel}), corrected by the potential battery power flow (P_{batt}) according to its direction:

$$\varepsilon_{real}(V_{veh}, a_{veh}, \omega_{in}, T_{in}) = -\frac{P_{out} + \left(\frac{1-\alpha}{2}\right) P_{batt}}{P_{fuel} + \left(\frac{1+\alpha}{2}\right) P_{batt}} \quad (19)$$

where $\alpha = sign(P_{batt})$. According to the positive sign of power flows indicated in Figure 1, $\alpha = 1$ for battery discharge ($P_{batt} > 0$, in input to the powertrain), while $\alpha = -1$ for battery recharge ($P_{batt} < 0$, in output).

The second performance index is derived from the power-weighted efficiency approach, which was proposed in [27–30] to consider the profoundly different working principles and performance of ICE and electric MGs.

The underpinning idea is that the actual efficiency of each actuator should be normalised to its maximum efficiency to fairly compare the performance of ICE and electric unit, given that ICE maximum efficiency is much lower than MGs one. The worse performance of the ICE is due to the fact that it converts the low-quality energy of the fossil fuel into mechanical energy; instead, the electric motors generate mechanical energy from high-quality electric energy, which, however, is usually obtained from the ICE operation, especially in FHEVs.

Thus, the fuel power of Eq. (17) and the battery power of Eq. (18) can be rearranged as follows:

$$P_{fuel}^{eq}(\omega_{in}, T_{in}) = \frac{\omega_{in} T_{in}}{\left(\frac{\eta_{ICE}}{\eta_{ICE,max}}\right)} \quad (20)$$

$$\begin{aligned} P_{batt}^{eq}&(V_{veh}, a_{veh}, \omega_{in}, T_{in}) \\ &= \bar{p}_o P_{in} \left(\frac{\eta_O}{\eta_{O,max}}\right)^{-sign(\bar{p}_o)} \\ &+ \bar{p}_i P_{in} \left(\frac{\eta_I}{\eta_{I,max}}\right)^{-sign(\bar{p}_i)} \end{aligned} \quad (21)$$

Thus, the equivalent efficiency is:

$$\varepsilon_{eq}(V_{veh}, a_{veh}, \omega_{in}, T_{in}) = -\frac{P_{out} + \left(\frac{1-\alpha_{eq}}{2}\right) P_{batt}^{eq}}{P_{fuel}^{eq} + \left(\frac{1+\alpha_{eq}}{2}\right) P_{batt}^{eq}} \quad (22)$$

where $\alpha_{eq} = sign\left(P_{batt}^{eq}\right)$. It should be noted that ε_{eq} does not have any physical meaning, in contrast to ε_{real}.

Moreover, the approach proposed in this paper differs from the power-weighted efficiency approach of [27–30] mainly because of the inclusion of mechanical power losses evaluation, which are neglected in [27–30].

3.3 CONSTRAINTS

After the calculation of the performance indices, only the feasible powertrain operations are eligible to become the optimal ones that maximise ε_{gl} or ε_{eq}. In other words, all the solutions violating the constraints on actuators speed, torque, and power should be excluded. The constraints on ICE operation are specified in Eq. (23); those on the MGs are in Eqs. (24)-(25):

$$\begin{aligned} &800 \text{ rpm} \le \omega_{in} \le 5800 \text{ rpm} \\ &T_{ICE,min}(\omega_{in}) \le T_{in}(\omega_{in}) \le T_{ICE,max}(\omega_{in}) \end{aligned} \quad (23)$$

$$\begin{aligned} &-10000 \text{ rpm} \le \omega_i \le 10000 \text{ rpm} \\ &T_{I,min}(\omega_i) \le T_i(\omega_i) \le T_{I,max}(\omega_i) \end{aligned} \quad (24)$$

$$\begin{aligned} &-10000\ rpm \le \omega_o \le 10000\ rpm \\ &T_{O,min}(\omega_o) \le T_o(\omega_o) \le T_{O,max}(\omega_o) \end{aligned} \quad (25)$$

Moreover, the battery power is constrained by the battery SOC. The boundary values depend on the instantaneous SOC, but the proposed static analysis cannot include such considerations. Therefore, four different scenarios for the battery SOC are simulated. In the first one (SOC = FREE), the battery can always provide or gather any power comprised between the lower and the higher values:

$$P_{max\_charge} \le P_{batt} \le P_{max\_discharge} \quad (26)$$

where $P_{max\_charge} = -70$ kW and $P_{max\_discharge} = 70$ kW. The condition whereby the battery is completely charged and thus prevented from receiving further power is indicated as SOC $= 1$ and implies $P_{max\_charge} = 0$. On the contrary, if the battery is fully discharged (SOC $= 0$), it cannot supply power and hence $P_{max\_discharge} = 0$. Lastly, the SOC can be maintained constant if $P_{batt} = 0$ (SOC=CONSTANT). Table II summarises SOC constraints.

Table II - SOC constraints.

SOC	P_{max_charge}	$P_{max\_discharge}$
FREE	-70 kW	70 kW
1	0	70 kW
0	-70 kW	0
CONSTANT	0	0

4 RESULTS AND DISCUSSION

The procedure described in Section 3 to assess the performance indices was implemented in MATLAB for a vehicle speed ranging from 0 to 200 km/h and a vehicle acceleration ranging from 0 to 2 m/s^2. A null road slope was considered ($\gamma = 0$ in Eq. (14)). However, the calculation can be repeated for any desired road slope. The mesh grid used in input to the script was derived by imposing $\omega_{in} = 800{:}\,10{:}\,5800$ rpm and $T_{in} = 20{:}\,1{:}\,167$ Nm.

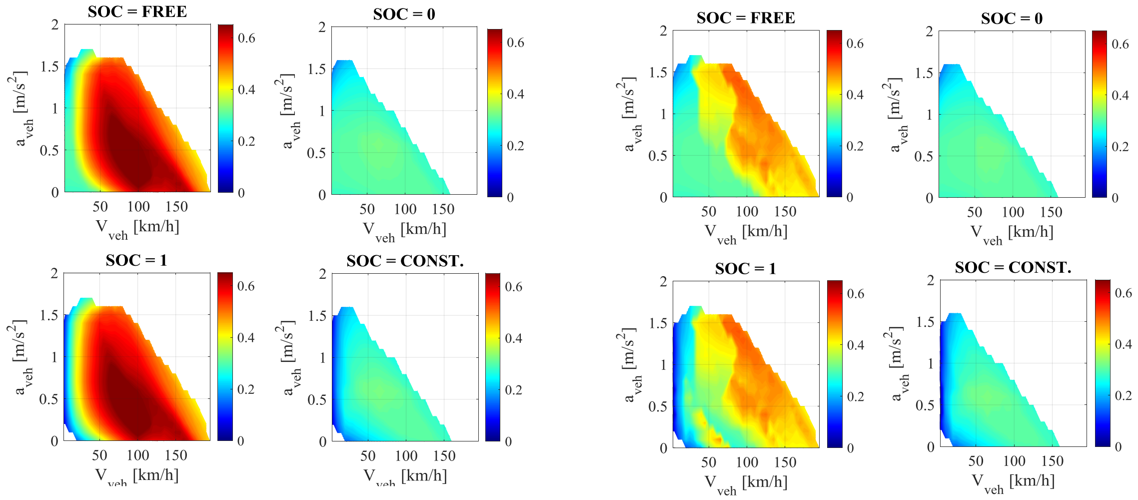

(a) (b)

Figure 6 Real global efficiency resulting from ε_{real} optimisation (a) and ε_{eq} optimisation (b).

For each combination of vehicle speed and acceleration, this section provides the optimal powertrain operations that maximise the real global efficiency or equivalent efficiency in terms of battery power and ICE and MGs functioning points.

Figure 6 shows a comparison between the optimal real global efficiency ε_{real} obtained by maximising the real global efficiency itself (Figure 6(a)) or the equivalent global efficiency ε_{eq} (Figure 6(b)). The optimisation of the two performance indices leads to different results. In particular, when the battery can provide electric energy (namely, in the scenarios SOC = FREE and SOC = 1), the optimisation of the equivalent efficiency significantly differs from the optimisation of the real global efficiency. This is due to the diverse utilisation of the engine (Figure 7) and battery power (Figure 8). The real powertrain global efficiency is optimised by minimising the ICE contribution to the propulsion (Figure 7(a)), or, in other words, by maximising the power supplied by the battery (Figure 8(a)) when possible, because of the much lower efficiency of the engine in comparison to the efficiency of the electric MGs. The minimisation of the ICE operation results in higher real global efficiency (Figure 6(a)). On the contrary, the equivalent efficiency is maximised when the engine operates within its most efficient region (Figure 7(b)); thus, less battery power is required for the traction, but surplus engine power is used for battery recharging (Figure 8(b)). However, the resulting real global efficiency is lower (Figure 6(b)).

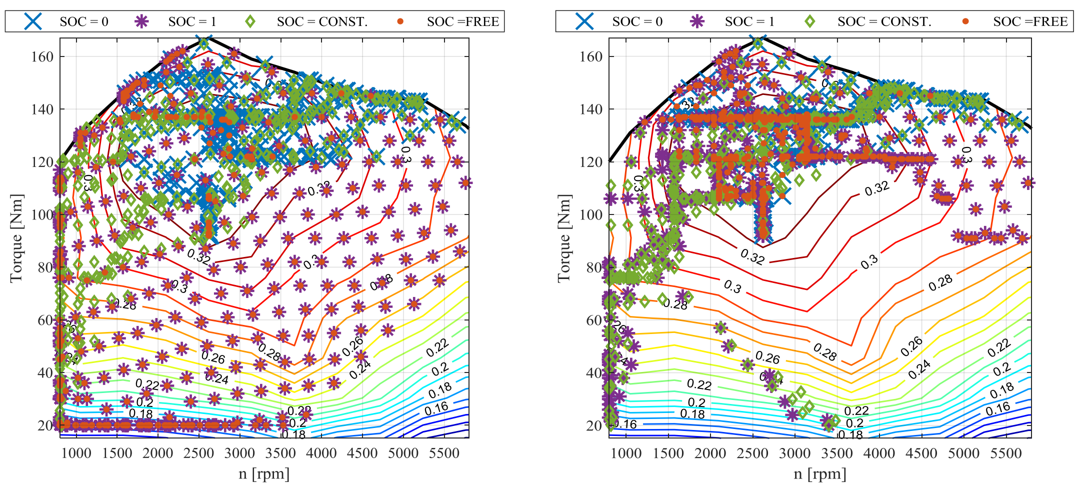

(a) (b)

Figure 7 ICE operation resulting from ε_{real} optimisation (a) and ε_{eq} optimisation (b).

These results suggest that the optimisation of the actual powertrain efficiency would lead to a long-term charge-depleting drive, while the maximisation of the equivalent efficiency would allow a charge-sustaining drive. Hence, the first approach would be more suitable for PHEVs, while the second for FHEVs that cannot be recharged from the grid.

A deeper analysis of the results in Figures 6-8 suggests a correlation between the trend of the highest real global efficiency achievable in each optimisation scenario by varying the constraints on the battery SOC. Indeed, in general, the real global efficiency is higher if the battery SOC is unconstrained ($SOC = FREE$).

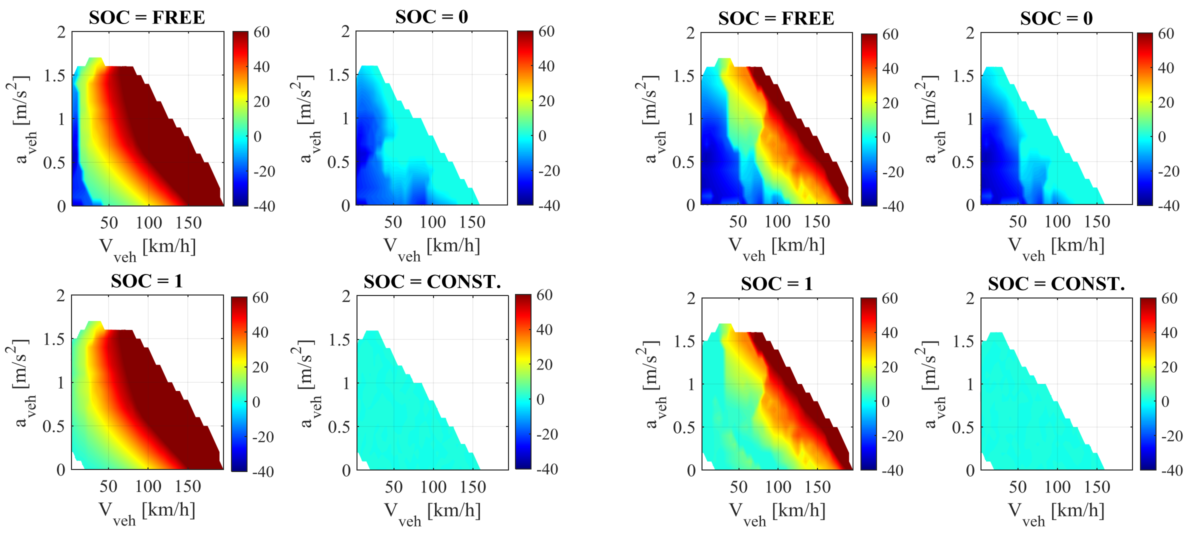

(a) (b)

Figure 8 Battery power ([kW]) resulting from ε_{real} optimisation (a) and ε_{eq} optimisation (b).

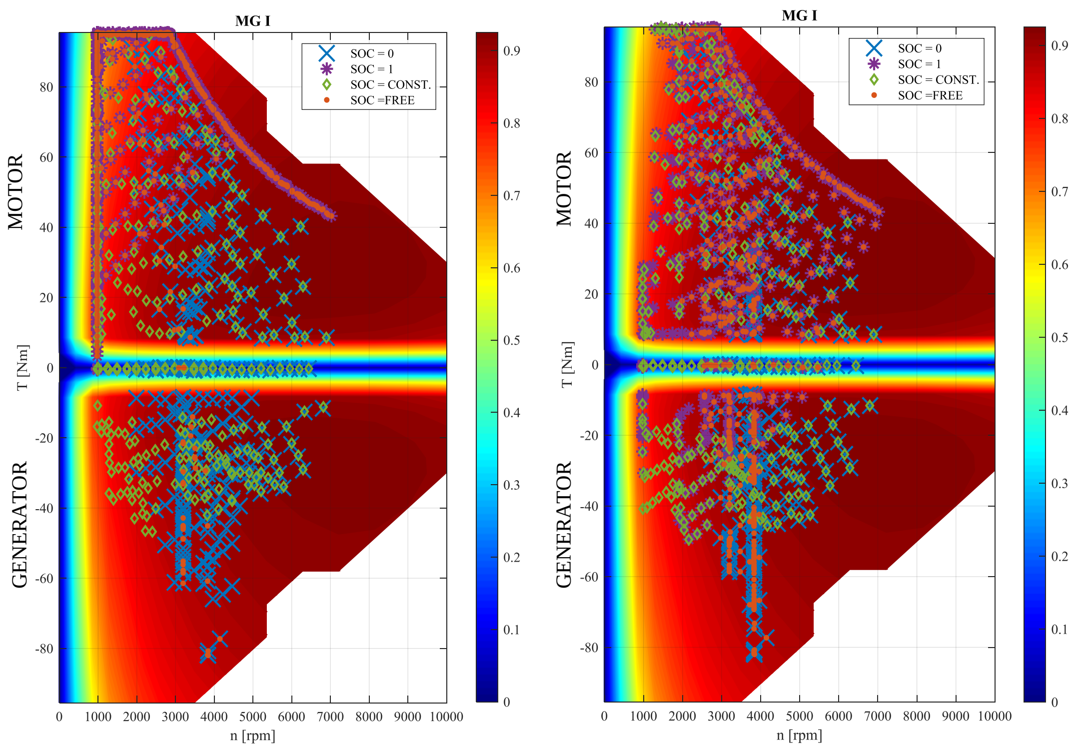

(a) (b)

Figure 9 MG I operation resulting from ε_{real} optimisation (a) and ε_{eq} optimisation (b).

If this result is obvious when the optimised index is the real global efficiency itself, it cannot be taken for granted when the equivalent efficiency is optimised, precisely because they are two different objective functions. Indeed, for a speed range of 30-75 km/h and low acceleration, the best global efficiency is achieved for $\mathrm{SOC} = 1$ and not for $\mathrm{SOC} = \mathrm{FREE}$ when the equivalent efficiency is optimized (Figure 6(b)). Moreover, both strategies output similar results when the battery is completely discharged ($\mathrm{SOC} = 0$) or a constant SOC is desired ($\mathrm{SOC} = \mathrm{CONSTANT}$). In this case, lower speeds and accelerations can be reached because the battery cannot support the engine for traction. Also, the ICE power increases for both optimisation strategies for high vehicle speeds and accelerations because the battery power would not be sufficient to provide the demanded power alone. Moreover, the condition whereby the ICE is turned off was not simulated; thus, low vehicle speeds and accelerations appear unfeasible for $\mathrm{SOC} = 1$ and $\mathrm{SOC} = \mathrm{CONSTANT}$ because the battery cannot gather the engine surplus power. Figure 9 and Figure 10 show the optimal operations of MG I and MG O, respectively. The functioning points of each MG are similar for $\mathrm{SOC} = 0$ and $\mathrm{SOC} = \mathrm{CONSTANT}$ for both optimisation strategies. Instead, they differ if $\mathrm{SOC} = \mathrm{FREE}$ and $\mathrm{SOC} = 1$, where both MG I and MG O are more exploited as generators when the equivalent efficiency is maximised (Figure 9(b) and Figure 10(b)). On the contrary, the optimisation of the real global efficiency requires more motoring operations (Figure 9(a) and Figure 10(a)), accordingly to the fact that more battery power is provided for vehicle propulsion.

Observing the ICE and MGs optimal speed, torque and power as functions of vehicle speed and acceleration (figures not reported here for brevity but deducible also from Figure 7, Figure 9 and Figure 10) turns out that only MG O is widely used at its maximum performance. In contrast, ICE is strongly underused for low vehicle speeds and accelerations if the real global efficiency is maximised. At the same time, MG I is rather underexploited if the equivalent efficiency is maximised. Indeed, the design of the transmission under analysis carried out in [26] aimed to potentially provide the maximum power to the wheels for any driving condition, even at low speed when it is not strictly required. No ICE and MGs efficiency map was considered during the design stage, nor an optimisation of any efficiency was pursued. Thus, a more efficiency-oriented design procedure could have led to different sizes of the actuators and powertrain performance.

Figure 11 shows the efficiency of ICE and MGs in each SOC scenario derived from the optimisation of the real global efficiency, while Figure 12 shows their efficiency leading to the optimisation of the equivalent efficiency. These results indicate the main difference between the two performance indices. Figure 12 shows that the optimisation of the equivalent efficiency leads to the maximisation of the efficiency of each power source, battery SOC notwithstanding.

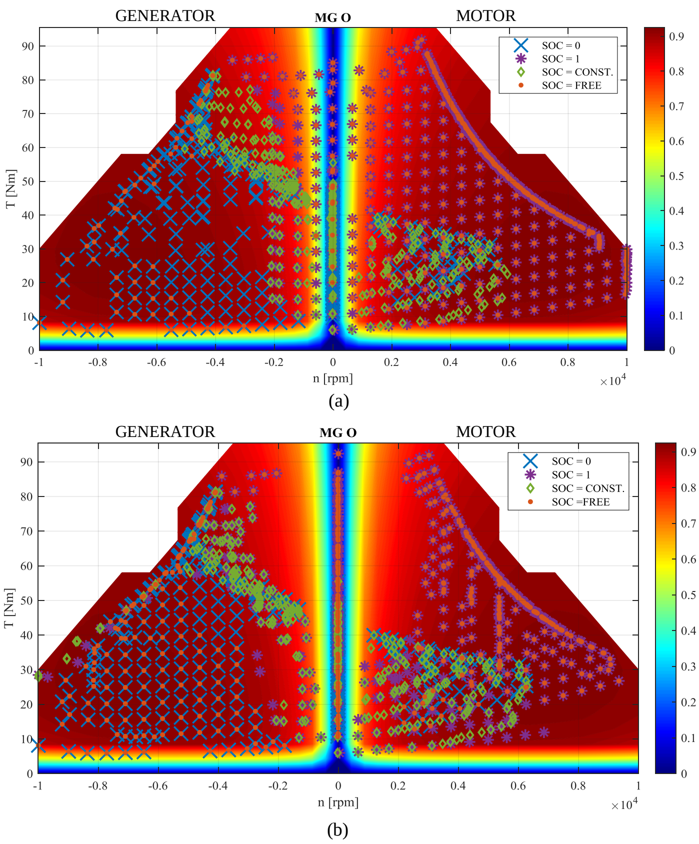

Figure 10 MG O operation resulting from ε_{real} optimisation (a) and ε_{eq} optimisation (b).

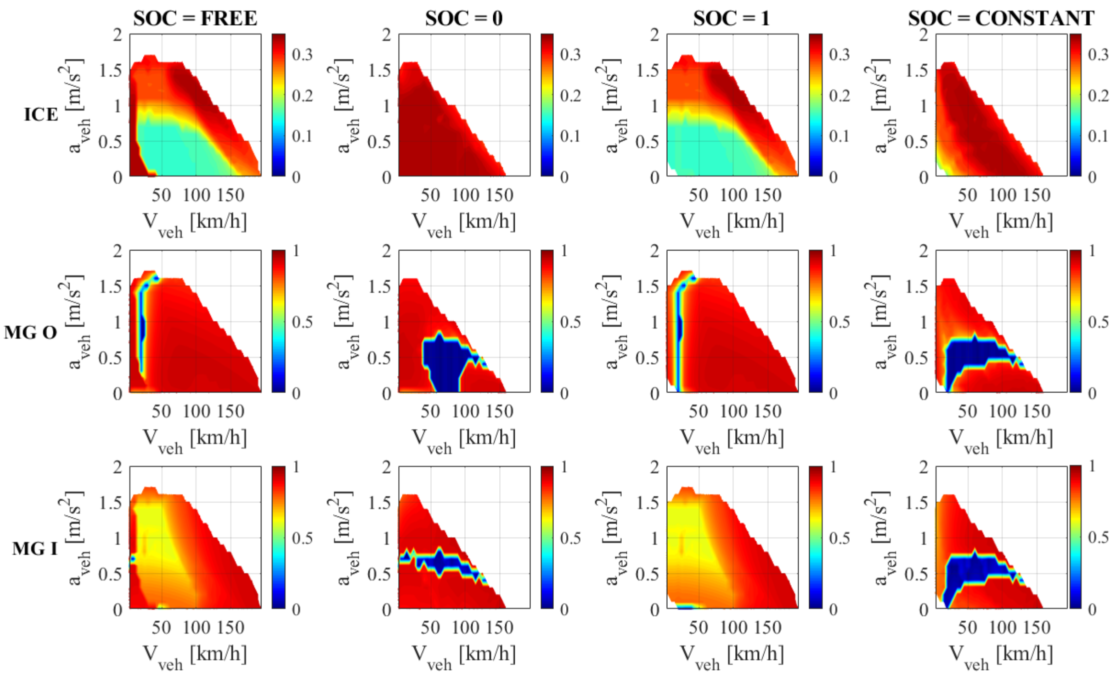

Figure 11 ICE, MG O and MG I efficiency resulting from ε_{real} optimisation.

On the contrary, the optimisation of the real global efficiency minimises the ICE power flows when the battery power is available, even though it has to work in a low-efficiency region. Nevertheless, for $SOC = 0$ and $SOC = CONSTANT$, both approaches maximise the actuators efficiency.

The zones where the MGs efficiency is zero in Figure 11 and Figure 12 are due to the fact that MG I is running without providing any torque, while MG O is stationary at its mechanical point.

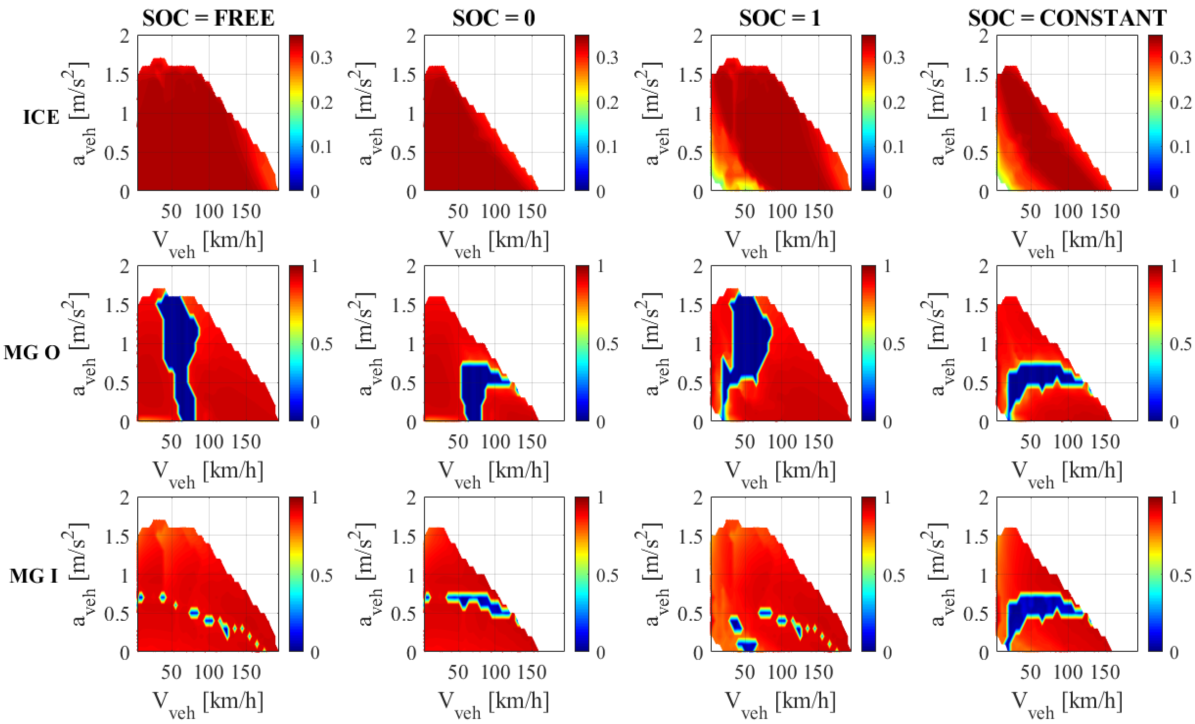

Figure 12 ICE, MG O and MG I efficiency resulting from ε_{eq} optimisation.

5 CONCLUSIONS

This work compared two performance indices to optimise a power-split hybrid electric powertrain. Their assessment was enabled by a procedure based on a unified parametric model suitable for any PS-CVT, which evaluates the mechanical power losses occurring in the transmission and the actual mechanical power required to the electric machines. The introduction of the road load and ICE and MGs efficiency maps led to a comprehensive analysis of the powertrain behaviour. Then, the operations leading to the maximisation of the performance indices were selected according to the constraints on ICE and MGs working range. Furthermore, constraints on the battery SOC were imposed to simulate four different simplified scenarios.

The considered performance indices were the real powertrain global efficiency and an apparent efficiency where ICE and MGs efficiency was normalised to the respective maximum value. The results suggested that considering the actual ICE efficiency, which is considerably lower than the MGs efficiency, would strongly penalise ICE operation, thus favouring battery power utilisation. However, this would lead to a charge-depleting drive that can suit PHEVs, not FHEVs. On the contrary, optimising the equivalent efficiency corresponds to maximising both ICE and MGs efficiency, thus resulting in a more charge-sustaining drive.

For a more accurate powertrain model, the ICE and electric MGs inertia should also be considered, which here was neglected. Future works can exploit this PSU model in a time-dependent simulation of the powertrain response by introducing reference drive cycles, so as to consider the instantaneous battery SOC and the regenerative braking to implement a robust energy management strategy.

REFERENCES

[1] Mi C. and Masrur M.A., *Hybrid Electric Vehicles: Principles and Applications with Practical Perspectives*, 2nd edition, John Wiley & Sons Ltd, 2017.

[2] Ehsani M., Gao Y., Gay S.E. and Emadi A., *Modern Electric, Hybrid Electric, and Fuel Cell Vehicles: Fundamentals, Theory, and Design*, CRC Press LLC, 2005.

[3] Krithika V. and Subramani C., A Comprehensive Review on Choice of Hybrid Vehicles and Power Converters. *Control Strategies for Hybrid Electric Vehicles Int. J. Energy Res*., Vol. 42, No. 5, pp. 1789–1812, 2018.

[4] Zhuang W., Li (Eben) S., Zhang X., Kum D., Song Z., Yin G. and Ju F., A Survey of Powertrain Configuration Studies on Hybrid Electric Vehicles. *Appl. Energy*, Vol. 262, p. 114553, 2020.

[5] Zeng X. and Wang J., *Analysis and Design of the Power-Split Device for Hybrid Systems*, Springer, Singapore, 2017.

[6] Wang L., Cui Y., Zhang F. and Li G., Architectures of Planetary Hybrid Powertrain System: Review, Classification and Comparison. *Energies*, Vol. 13, No. 2, 2020.

[7] Onori S., Serrao L. and Rizzoni G., *Hybrid Electric Vehicles Energy Management Strategies*, Springer, London, 2016.

[8] Zhang P., Yan F. and Du C., A Comprehensive Analysis of Energy Management Strategies for Hybrid Electric Vehicles Based on Bibliometrics. *Renew. Sustain. Energy Rev.*, Vol. 48, No. 205, pp. 88–104, 2015.

[9] Martinez C. M., Hu X., Cao D., Velenis E., Gao B. and Wellers M., Energy Management in Plug-in Hybrid Electric Vehicles: Recent Progress and a Connected Vehicles Perspective. *IEEE Trans. Veh. Technol.*, Vol. 66, No. 6, pp. 4534–4549, 2017.

[10] Sforza A., Lenzo B. and Timpone F., A State-of-the-Art Review on Torque Distribution Strategies Aimed At Enhancing Energy Efficiency for Fully Electric Vehicles with Independently Actuated Drivetrains. *Int. International Journal of Mechanics and Control*, Vol. 20, No. 02, pp. 3–15, 2019.

[11] Zhang F., Wang L., Coskun S., Pang H., Cui Y. and Xi J., Energy Management Strategies for Hybrid Electric Vehicles: Review, Classification, Comparison, and Outlook. *Energies*, Vol. 13, No. 13, pp. 1–35, 2020.

[12] Sabri M.F.M., Danapalasingam K.A. and Rahmat M.F., A Review on Hybrid Electric Vehicles Architecture and Energy Management Strategies. *Renew. Sustain. Energy Rev.*, Vol. 53, pp. 1433–1442, 2016.

[13] Silvagni M., Chiaberge M. and Tessari F., UAV Powertrain Efficient Design through a Model-Based Approach. *International Journal of Mechanics and Control*, Vol. 19, No. 01, pp. 15–22, 2018.

[14] Spano M., Del Vescovo D., Sangeorzan B., Misul D. and Belingardi G., Optimizing Engine Downsizing and Driving Behaviour in Conventional and Hybrid Powertrains for Autonomous Driving Applications. I*nt. J. Mech. Control*, Vol. 21, No. 02, pp. 1–12, 2020.

[15] Zhang F., Hu X., Langari R. and Cao D., Energy Management Strategies of Connected HEVs and PHEVs: Recent Progress and Outlook. *Prog. Energy Combust. Sci.*, Vol. 73, pp. 235–256, 2019.

[16] Berri P.C., Dalla Vedova M.D.L., Maggiore P. and Manuello Bertetto A., Simplified Models for Mechanical Transmission Efficiency with Opposing and Aiding Loads. *International Journal of Mechanics and Control*, Vol. 20, No. 02, pp. 135–139, 2019.

[17] González-Cruz C.A., Ceccarelli M., Jáuregui-Correa J.C. and Alimehmeti M., An Experimental Characterization of a Two-Stage Planetary Gear Transmission under Non-Stationary Operation. *International Journal of Mechanics and Control*, Vol. 22, No. 01, pp. 115–124, 2021.

[18] Cammalleri M. and Sorge F., Approximate Closed-Form Solutions for the Shift Mechanics of Rubber Belt Variators. *Proc. ASME Int. Des. Eng. Tech. Conf. Comput. Inf. Eng. Conf. 2009*, DETC2009-86638, pp. 187–196, 2010.

[19] Zhu Y., Li X., Liu Q., Li S. and Xu, Y., A Comprehensive Review of Energy Management Strategies for Hybrid Electric Vehicles. *Mech. Sci.*, Vol. 13, No. 1, pp. 147–188, 2022.

[20] Cammalleri M. and Rotella D., Functional Design of Power-Split CVTs: An Uncoupled Hierarchical Optimized Model. *Mech. Mach. Theory*, Vol. 116, pp. 294–309, 2017.

[21] Rotella D. and Cammalleri M., Direct Analysis of Power-Split CVTs: A Unified Method. *Mech. Mach. Theory*, Vol. 121, pp. 116–127, 2018.

[22] Rotella D. and Cammalleri M., Power Losses in Power-Split CVTs: A Fast Black-Box Approximate Method. *Mech. Mach. Theory*, Vol. 128, pp. 528–543, 2018.

[23] Cammalleri M. and Castellano A., Analysis of Hybrid Vehicle Transmissions with Any Number of Modes and Planetary Gearing : Kinematics, Power Flows, Mechanical Power Losses. *Mech. Mach. Theory*, Vol. 162, p. 104350, 2021.

[24] Castellano A. and Cammalleri M., Global Efficiency of Power-Split Hybrid Electric Powertrain. *Quaglia G., Gasparetto A., Petuya V., Carbone G. (eds) Proceedings of I4SDG Workshop 2021. I4SDG 2021. Mechanisms and Machine Science*, Vol. 108. Springer, Cham., pp. 502–511, 2022.

[25] Castellano A. and Cammalleri M., Power Losses Minimization for Optimal Operating Maps in Power-Split Hevs: A Case Study on the Chevrolet Volt. *Appl. Sci.*, Vol. 11, No. 17, p. 7779, 2021.

[26] Rotella D., Cammalleri M., Qin D. and Zhou X., A Simple Method for the Design of Hybrid Electric Power-Split Cvts: A Case Study. *Springer International Publishing*, 2019.

[27] Zhang X., Peng H. and Sun J., A Near-Optimal Power Management Strategy for Rapid Component Sizing of Multimode Power Split Hybrid Vehicles. *IEEE Trans. Control Syst. Technol.*, Vol. 23, No. 2, pp. 609–618, 2015.

[28] Zhang X., Eben Li S., Peng H. and Sun J., Efficient Exhaustive Search of Power-Split Hybrid Powertrains with Multiple Planetary Gears and Clutches. *J. Dyn. Syst. Meas. Control. Trans. ASME*, Vol. 137, No. 12, 2015.

[29] Tota A., Galvagno E. and Velardocchia M., On the Power-Weighted Efficiency of Multimode Powertrains: A Case Study on a Two-Mode Hybrid System. *Quaglia G., Gasparetto A., Petuya V., Carbone G. (eds) Proceedings of I4SDG Workshop 2021. I4SDG 2021. Mechanisms and Machine Science,* Vol. 108. Springer, Cham., pp. 522–531, 2022.

[30] Tota A., Galvagno E., Dimauro L., Vigliani A. and Velardocchia M., Energy Management Strategy for Hybrid Multimode Powertrains: Influence of Inertial Properties and Road Inclination. *Appl. Sci.*, Vol. 11, No. 24, p. 11752, 2021.